

---

# CONNECTING THE DOTS: RANGE EXPANSIONS ACROSS LANDSCAPES WITH QUENCHED NOISE

---

Jimmy Gonzalez Nuñez<sup>1</sup>, Jayson Paulose<sup>2</sup>, Wolfram Möbius<sup>3,4</sup>, and Daniel A. Beller<sup>1</sup>

<sup>1</sup>Department of Physics and Astronomy, Johns Hopkins University, Baltimore, MD

<sup>2</sup>Department of Physics and Institute for Fundamental Science, University of Oregon, Eugene, OR

<sup>3</sup>Living Systems Institute, Faculty of Health and Life Sciences, University of Exeter, Exeter, UK

<sup>4</sup>Physics and Astronomy, Faculty of Environment, Science and Economy, University of Exeter, Exeter, UK

October 19, 2023

## ABSTRACT

---

When biological populations expand into new territory, the evolutionary outcomes can be strongly influenced by genetic drift, the random fluctuations in allele frequencies. Meanwhile, spatial variability in the environment can also significantly influence the competition between sub-populations vying for space. Little is known about the interplay of these intrinsic and extrinsic sources of noise in population dynamics: When does environmental heterogeneity dominate over genetic drift or vice versa, and what distinguishes their population genetics signatures? Here, in the context of neutral evolution, we examine the interplay between a population's intrinsic, demographic noise and an extrinsic, quenched-random noise provided by a heterogeneous environment. Using a multi-species Eden model, we simulate a population expanding over a landscape with random variations in local growth rates and measure how this variability affects genealogical tree structure, and thus genetic diversity. We find that, when the heterogeneity is sufficiently strong, the population front is dominated by genealogical lineages that are pinned to a small number of optimal paths. The landscape-dependent statistics of these optimal paths then supersede those of the population's intrinsic noise as the main determinant of evolutionary dynamics. Remarkably, the statistics for coalescence of genealogical lineages, derived from those deterministic paths, strongly resemble the statistics emerging from demographic noise alone in uniform landscapes. This cautions interpretations of coalescence statistics and raises new challenges for inferring past population dynamics.

---

## Introduction

these footprints, it is important to understand how they originated. Range shifts are now understood to be common to many population histories [1], from small scale bacterial colonies [2, 3, 4] and cancerous tissues [5, 6, 7] to large scale species invasion in foreign biomes [8, 9] and human migration [10, 11, 12, 13]; they thus play an important role in connecting evolution and ecology [14, 15].

Large, well-mixed populations are insensitive to intrinsic, random genetic fluctuations, i.e., genetic drift. In contrast, during range expansions, “luck” plays a significant role in providing rare, neutral mutations an opportunity to rise to high frequency and appreciably contribute to the expanding population [16, 17, 18, 19]. This increased influence of genetic drift arises because evolutionary competition becomes restricted to small effective population sizes at the boundaries between isogenic groups. As a result, local genetic diversity decreases rapidly with increasing expansion distance [20, 21, 22, 23].

In the absence of long-range dispersal, genetic diversity at a traveling population front can be characterized by the motion of boundaries separating regions of similar genetic makeup, as well as by branching genealogical lineage trees caused by repeated founder effects [24]. When viewed backward-in-time, genetic dynamics are characterized by the intersections and coalescences of the population’s genetic lineages, traced from the population front back to the location of the initial populations. Along the way, pairs of related lineages sampled from the front eventually coalesce in a most recent common ancestor. The time since this coalescence event is then proportional to the number of accumulated (neutral) mutations expected to distinguish the genomes of the two sampled organisms, providing an important measure of genetic diversity [25, 26] and coupling the non-equilibrium statistics of propagating fronts to population genetics.

Little is known about how environmental heterogeneity interacts with this decay of genetic diversity and shapes the evolutionary outcome. Such an interplay has potential ecological and evolutionary consequences, e.g., the emergence of antibiotic resistance [4] and altered species invasion dynamics [27, 28]. Some progress has been made in understanding statistics of relatedness across the landscape in bounded environments [29], for single obstacles to the expansion [30], and for environments with curved surfaces [31]. In particular, individual obstacles, which suppress growth locally, act similarly to bumps in surface topography by focusing the expansion front inward to a cusp [30, 31]. Landscapes of randomly placed obstacles create pinning sites for the population front and increase the importance of chance relative to selective fitness in determining the genetic makeup of the expansion [32].

However, it remains poorly understood how a heterogeneous growth landscape influences the genetic structure

of expanding populations. To study this interplay, we examine the effects of environmental heterogeneity on a minimal model of population growth, the multi-species Eden model [33], in which the front of the range expansion is a propagating, roughening interface in the Kardar-Parisi-Zhang (KPZ) universality class [34]. Motivated by experiments on bacterial and yeast colonies grown on agar plates with limited nutrients [20, 17, 35, 36, 22], the evolutionary dynamics of this model in uniform environments has been extensively studied, including phenomena such as fitness collapse [37, 38], fixation [39], gene surfing [40, 22], and genetic lineage coalescence [41, 32].

In this work, we couple the Eden model’s range expansion to a landscape of *hotspots* where the population expands faster locally. The effects of hotspots, both individually and in randomly placed collections, have recently been characterized by employing an analogy of light rays passing through a medium of regions with locally decreased index of refraction [42]. We demonstrate that for strong heterogeneity, despite appearing stochastic, the population’s genetic lineage structure is dominated by geometrically determined paths of least travel time, and these paths predict which initial sub-populations will dominate the late stages of the expansion. Strikingly, we find that strong environmental noise can produce statistics in the population’s genetic composition that mimic scaling due to demographic noise on uniform landscapes, despite making the genetic outcomes nearly deterministic.

## Model

Our simulated population is arranged on a hexagonal grid, with each filled grid site containing a *deme* (well-mixed sub-population) that can grow or expand into neighboring sites (Fig. 1A). In the context of a continuous population, this corresponds to the regime where growth to local carrying capacity occurs faster than migration. For this reason, the genetic character of each deme is assumed to be uniquely determined by the first individual to arrive. We consider reproduction of demes to occur only at the population boundary, i.e., no replacement of an occupied deme is possible, leading to a population composition that is “frozen” in time. In this scenario, we can use a single identifier to characterize the local genetic composition, which we represent with a distinct color (Fig. 1A).

Our initial condition consists of a single, filled edge of  $L$  sites on our hexagonal grid (Fig. 1A). We choose each initially occupied site to be identified with one of  $L$  colors with all demes sharing equal intrinsic fitness (neutral evolution). We employ asynchronous reproduction rules known to reproduce the scaling (discussed in more detail later) of domain boundary fluctuations [20] and genetic lineage lateral motion [22] often seen in microbial experiments, as well as many classes of systems with kinetically roughened fronts [43].

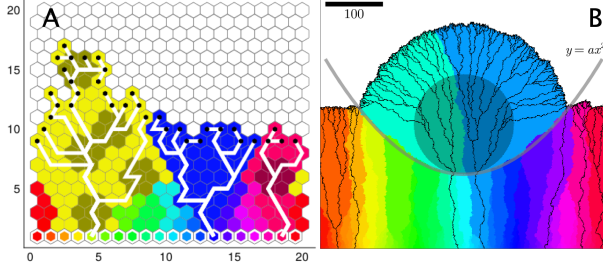


Figure 1: Illustration of Eden model for a range expansion on a heterogeneous landscape of hotspots with a linear inoculation initial condition (white-outlined hexagon markers), and with each color representing a distinct ancestral deme. Gray sites make up the *hotspots*, regions of increased reproduction rate. (A) Simulation showing genetic lineages (white lines) at the scale of the lattice and intensity  $I = 9$ . Black dots highlight the population front. (B) Simulation showing the effect of a single hotspot on the genetic lineages (black lines) and population front, using intensity  $I = 9$ . Parabolic approximation to the sector boundaries induced by the hotspot is shown in gray.

These reproduction rules consist of (1) identifying the population front by all demes near an empty grid site, (2) randomly selecting one deme at the population front according to an implementation of the Gillespie algorithm [44, 45], and (3) randomly selecting one neighboring grid site with uniform probability to establish a new deme of the same color as the replicating deme. For neutral evolution in uniform environments, this amounts to selecting individual demes at the front with equal probability and copying their color to a random adjacent empty site, *c.f.* Eden model [33], type C [46]. Because color is inherited at replication, this process leads to single-colored regions, each occupied by descendants of one individual from the original population (Fig. 1A). By tracking replications, we can also visualise the ancestral relationships between sites. Here, we focus on the ancestral history of individuals at the front, which are represented by lineages that coalesce when viewed backwards in time (white lines in Fig. 1A).

Environmental heterogeneity in our system takes the form of a fixed distribution of disk-shaped “hotspots”, which are regions of increased local reproduction rate (Fig. 1). Thus, for heterogeneous environments, step (2) is modified first by assigning to each grid site  $(i, j)$  a reproduction rate,

$$r(i, j) = \begin{cases} r_h & \text{if } (i, j) \text{ in a hotspot,} \\ r_0 & \text{otherwise,} \end{cases} \quad (1)$$

where  $r_h, r_0$  are the reproduction rates inside and outside of a hotspot, respectively. Thus, reproduction occurs through an implementation of the Gillespie algorithm: for a population front consisting of  $n_h$  demes in hotspots and  $n_0$  demes outside of hotspots, the probability of selecting

a particular deme inside of a hotspot as the next site to reproduce is  $P_h = r_h/Q$  with  $Q = n_h r_h + n_0 r_0$  being the sum of reproduction rates of demes at the front. After replication, time is updated according to the Gillespie algorithm by  $\delta t = -\log(\eta)/Q$ , with  $\eta$  being a uniform pseudo-random number in the range  $[0, 1]$  [44]. A single disk-shaped hotspot leads to an expanding population bulge, as characterized in Ref. [42] (Fig. 1B).

Our structured environment takes the form of a “landscape” of hotspots with Poisson-distributed centers. The hotspots include all lattice sites centered within a distance  $R$  of any hotspot center and distance  $R$  away from the boundaries, and with overlap allowed between neighboring hotspots. This gives rise to three system parameters: the hotspot radius  $R$ , the area fraction  $\phi$  of hotspots, and the ratio of replication rates  $r_h/r_0$ . The latter parameter can be recast as the hotspot intensity,  $I = (r_h/r_0) - 1$ . Because the replication rate is proportional to front speed, hotspot intensity can be rewritten as  $I = (v_h/v_0) - 1$  which  $v_h$  and  $v_0$  being front speed within and outside the hotspots, respectively.

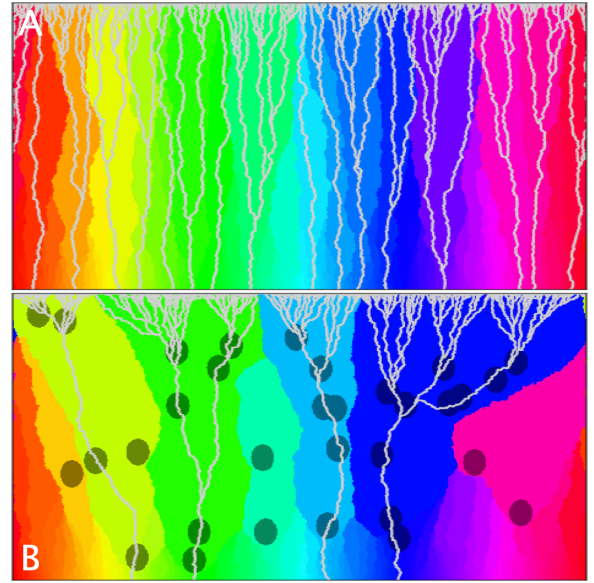


Figure 2: Illustration of a range expansion from a linear initial population of 2000 demes wide grown to 1000 demes tall showing sector coarsening (colors) and genetic lineage structure (light gray trails), (A) without hotspots, and (B) with hotspots (dark gray disks) at an area fraction  $\phi = 0.09$ , radius  $R = 20$  and intensity  $I = 7$ .

Simulations are performed on a hexagonal grid with periodic boundaries along the width direction, and beginning with initial populations of  $L$  demes. Our simulated population is grown only to a height of  $L/2$  demes to reduce finite size effects in genetic measures by preventing genetic lineages from self-interacting. Specifically, viewed forward in time, replicating demes which happen to establish new demes consistently in one direction will have descendent demes that have been displaced at

most a distance equal to half the system width. Viewed backward-in-time, then, genetic lineages constructed by tracing these replication events backwards from demes at the population front toward a founding ancestor do not have enough time to wrap through the periodic boundaries onto themselves.

## Results

### Effect of a single-hotspot on genetic diversity

Expansion of the population on the lattice leads to a loss of genetic diversity, which can be seen in the decrease in the number of distinct colors with increasing height, Fig. 1A. Occasionally a deme of a particular color will be surrounded by demes of other colors, preventing it from establishing new descendants; two sector boundaries then merge into one. Since a merger of boundaries results in the termination of genetic lineages contained within one of these genetic sectors, such sector coarsening is strongly coupled to genetic lineage structure. That is, decreases in the number of genetic sectors also correspond to a decrease in the number of founder-population ancestors that “survive”, *i.e.* that remain present as distinct roots of genetic lineage trees (white lines in Fig. 1A, gray lines in Fig. 2) traced backward from the population front. This has been studied extensively in uniform environments; the number of surviving sectors and genetic lineages admit KPZ scaling [20, 22].

Fig. 1B shows a range expansion at a scale much larger than the lattice spacing with a single hotspot at the center of the landscape with intensity  $I = 9$ . Descendants of demes at the population front entering the hotspot are rapidly directed to the hotspot periphery. The front propagation there can be understood as a superposition of a traveling plane wave and a spherical wave whose intersection traces out a parabola, consistent with Eikonal equation solutions recently found for hotspots [42], with the subtle difference that here the parabola’s vertex occurs a distance  $IR/(I + 1)$  below the hotspot center (see **SI Appendix**). The outward-biased motion of sector boundaries induced by the hotspot results in a rapid reduction in the number of sectors in the vicinity of the hotspot. This means that those unlucky few lineages that pass near the hotspot without entering it will very likely be cut off by the parabolic sector boundary formed. As shown in Fig. 1, the parabolic sector boundary follows  $y = ax^2$ , with origin at the base of the hotspot and with coefficient

$$a = (1 + I)/(4IR) \quad (2)$$

calculated from geometric optics [42]. For high hotspot intensity, the parameter  $a$  saturates to  $1/(4R)$ , suggesting that each hotspot contributes to accelerated genetic diversity loss over an effective range of influence of order  $4R$ .

For lineages, the hotspot acts like a diverging lens (viewed from bottom to top, Fig. 1B). This is in contrast to obstacles and topographic bumps where lineages are

guided around the environmental feature like a converging lens focuses light [31, 42]. For topographic bumps it was shown that average lineage trajectories are well predicted by analytically calculated geodesic paths [31], *i.e.*, the paths of least time. In this work, we therefore expect fastest paths through a landscape of many hotspots to provide useful predictions for trajectories of surviving lineages. We investigate this hypothesis in detail below, in **Least Time Principle and Genetic Lineage Structure and Meandering of Lineages and of Fastest Paths**.

### Many-hotspot effects on diversity

While a single hotspot has a qualitatively simple geometrical effect on front geometry, sector coarsening, and shape of lineages, the situation is complicated in the presence of many hotspots. It is known that the shape of the advancing population front remains well described by geometric optics calculations for paths of least time [42]. Here, we investigate the consequences that landscapes of many hotspots have on the population’s genetic diversity.

Example simulations for a range expansion through a uniform landscape ( $\phi = 0$ ), and a landscape with hotspot area fraction  $\phi = 0.09$ , hotspot size  $R = 10$ , and intensity  $I = 9$  are shown in Figures 2A,B respectively. Comparing these two figures shows that landscapes of many hotspots qualitatively hasten genetic sector coarsening, resulting in a corresponding drop in the number of surviving genetic lineages, and leading to greater lateral meandering in both genetic lineages and sector boundaries.

### Sector coarsening

To study the decay in the number  $n_s$  of genetic sectors, we measure how the average sector width  $l_s(\bar{h}) \sim 1/n_s$  grows as a function of the average front height (expansion distance)  $\bar{h}$  (Fig. 3). In the absence of hotspots, there is experimental [20] and numerical [47] evidence of a scaling relation  $l_s \sim \bar{h}^\gamma$ , with  $\bar{h}$  being expansion distance from initial population and approximate KPZ scaling exponent of  $\gamma \approx 2/3$ . In agreement with this expectation, we find that the uniform-landscape cases ( $I = 0$  in Figure 3A,  $\phi = 0$  in Figure 3B) exhibit KPZ scaling  $l_s \sim \bar{h}^\gamma$ ,  $\gamma = 2/3$  for all heights beyond some initial height on the order 10 demes.

We explore how  $l_s(\bar{h})$  changes with two parameters describing the many-hotspot landscape: hotspot intensity  $I$  (Fig. 3A) and hotspot area fraction  $\phi$  (Fig. 3B). Tuning  $I$  from 0 to 1 results in a transient regime at heights  $\bar{h} \gtrsim 100$  which deviates from the uniform landscape case, and where sector size grows faster than  $\sim \bar{h}^{2/3}$ . After this transient regime, at high  $\bar{h}$ , sector growth returns to the KPZ scaling  $\gamma = 2/3$ , but with a prefactor that is greater for larger hotspot intensities (Fig. 3A). We see similar behavior when varying  $\phi$ , with the return to the

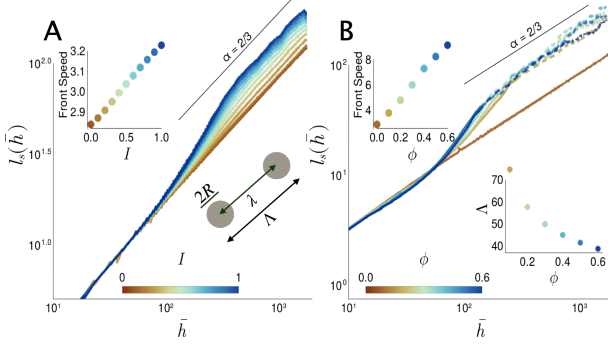


Figure 3: Log-log plot of the average genetic lateral sector size  $l_s$  plotted against mean expansion distance  $\bar{h}$  with radius  $R = 10$  and (A) varying hotspot intensity  $I$  at fixed density  $\phi = 0.09$ , (B) varying hotspot density  $\phi$  at fixed intensity  $I = 3$ . The hotspot radius is fixed at  $R = 10$ . Top-left insets show population front mean speed as a function of (A) hotspot intensity and (B) hotspot area fraction. Bottom-right insets show (A) schematic of hotspot typical outer-edge-to-outer-edge distance  $\Lambda$ , (B)  $\Lambda(\phi)$ . Dashed lines indicate  $l_s$  values above the corresponding  $\Lambda$  values from bottom-right inset in (B).

KPZ regime at high  $\bar{h}$  occurring slightly faster for higher area fractions (Fig. 3B).

For landscapes of many hotspots, previous work characterized front propagation by an effective front speed, approximating the heterogeneous landscape as a uniform, effective medium [42]. This effective front speed increases with both hotspot intensity  $I$  and area fraction  $\phi$  (Fig. 3A and B top-left inset). In this light, the return to KPZ scaling at large  $\bar{h}$  can be understood as signalling a regime where the effective medium description is valid, at expansion distances larger than some crossover length. To understand the transient behavior and the return to KPZ scaling at large expansion distance, we define a length scale for the typical hotspot center-to-center distance,  $\lambda \equiv 1/\sqrt{\rho}$ , where  $\rho$  is the hotspot number density. For a random distribution of discs permitted to overlap, this length is related to the hotspot area fraction  $\phi$  and radius  $R$  through [48, 49]

$$\lambda(\phi, R) \equiv \frac{1}{\sqrt{\rho}} = \sqrt{\frac{\pi R^2}{-\ln(1-\phi)}}. \quad (3)$$

Empirically, we find that the crossover length is well described by the typical outer-edge-to-outer edge distance  $\Lambda \equiv \lambda + 2R$  between nearby hotspots (Fig. 3A inset). Values for  $\Lambda$  calculated using Eq. 3 are shown in Fig. 3B inset for corresponding values of  $\phi$ . Those  $\Lambda$  values (represented by the transition from solid to dashed lines in Fig. 3B) provide fairly good approximations for the crossover  $\bar{h}$ -values at which sector size growth  $l_s(\bar{h})$  returns to KPZ scaling. This supports the effective medium picture for expansion distances larger than the

typical outer-edge-to-outer-edge distance between nearby hotspots. Thus, the transient regime leads to accelerated loss in genetic diversity.

### Environmentally Pinned Genetic Lineages

As described above, at sufficiently large expansion distances, genetic sector coarsening in many-hotspot landscapes scales similarly to that on uniform landscapes. Since the sector dynamics and genetic lineage structure are related, it would be reasonable to expect similar stochastic behaviour for genetic lineages. Indeed, individual simulations, such as Fig. 2B, may at first seem to indicate that growth through a landscape of hotspots produces genetic lineage trees similar to those in uniform environments, although with front roughening and sector coarsening accelerated by hotspots.

However, at close inspection, comparison of simulation runs from different initial random seeds but within the same landscape and initial condition reveals a qualitatively distinct feature of range expansions in landscapes with quenched random noise: When the hotspot intensity is sufficiently large, a large proportion of the genetic lineages follow certain highly traversed paths through a given landscape, traveling through a small, consistent subset of the hotspots. We dub this phenomenon *lineage pinning*. This effect is seen by averaging the genetic lineage spatial positions from 1200 simulations so that each lattice site records a probability of being visited by a surviving genetic lineage. Fig. 4A shows such a lineage site-visitation probability map for a uniform environment, with darker colors indicating more commonly visited positions. The observed texture arises from a finite ensemble of simulations; for an infinite ensemble in a uniform environment, all positions at a given height would be visited equally, by symmetry. In a heterogeneous landscape, a very different pattern emerges in Fig. 4B where the presence of hotspots induces a clear structure of frequently traversed positions passing through a subset of the hotspots.

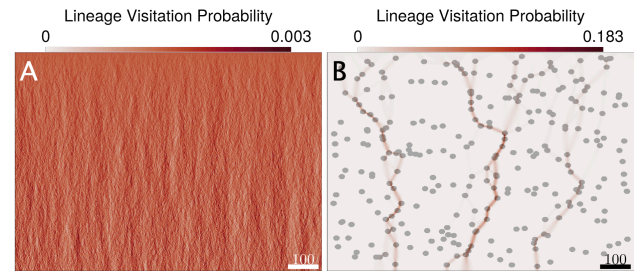


Figure 4: Genetic lineage site-visitation probability map averaged over an ensemble of 1200 simulations and number of lineages with (A) no hotspots and (B) a fixed landscape of hotspots with an intensity  $I = 3$ , size  $R = 10$ , and area fraction  $\phi = 0.09$ .

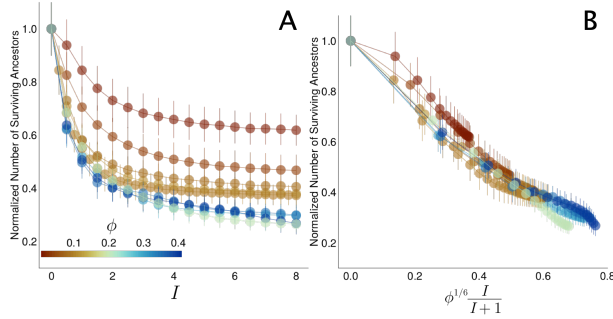


Figure 5: Normalized number of surviving ancestors after a range expansion as a function of: (A) hotspot intensity,  $I$ , for fixed radius  $R = 10$ ; (B) pinning parameter  $\phi^{1/6} I / (I + 1)$ . Color bar indicates area fraction  $\phi$  for each set of points. Error bars represent standard deviations.

With the front at the end of the simulation consisting of  $L$  demes by construction, the average genetic lineage tree pattern in Fig. 4B would indicate that there is a funneling of lineages to a reduced number of paths through the landscape, ultimately terminating on a finite subset of ancestral demes (located at height zero). This suggests that structured environments induce favorable paths for genetic lineages and thus impart a deterministic component to the evolutionary dynamics: the pattern of hotspots biases the genetic composition of the expansion front in favor of certain founding demes. In the forward-time view, this also implies deterministic contributions to genetic sector survival and dynamics of sector boundaries. The onset of lineage pinning is thus mediated by hotspot intensity: as  $I$  is increased, paths of high visitation probability emerge and become narrower as they accumulate more of the total probability.

Lineage pinning accelerates the decay of genetic diversity, as seen in a reduction in the number of surviving ancestors, *i.e.*, ancestral demes contributing to the front’s genetic makeup. As one summary statistic from these simulation ensembles, Fig. 5A displays the mean number of surviving ancestors (number of genetic tree roots), normalized by the corresponding number in the absence of hotspots, as a function of hotspot intensity. Values are smaller than 1, indicating that lineage pinning by the environment reduces the number of distinct roots exhibited by a given lineage tree. This effect saturates at high hotspot intensity. This saturating behavior is presumably related to the saturation of the prefactor in the parabola describing the effect of an isolated hotspot (Eq. 2); we speculate that a role is also played by the finite number of fastest paths through the landscape, as we discuss below. The  $\phi$ -dependence can be approximately collapsed by plotting the normalized number of surviving ancestors against  $\phi^{1/6} I / (I + 1)$ , where the  $I$ -dependence is motivated by Eq. 2 and the power of  $\phi$  is found empirically, as shown in Fig. 5B.

Thus, we find that heterogeneous landscapes can accelerate loss of genetic diversity and yet produce sector coarsening statistics that, at late times, resemble statistics in uniform landscapes.

### Least Time Principle and Genetic Lineage Structure

The geometry of an advancing population front in a landscape of hotspots can be understood in analogy with light rays propagating through a heterogeneous medium, with hotspots effectively behaving as diverging lenses [42]. Building on this analogy, we demonstrate here that geometrically determined paths of least travel time through a landscape of hotspots predict much of the observed genetic lineage structure in range expansions, including which founding ancestors will have surviving descendants.

We determine these shortest travel time paths on our discretized landscape using the Dijkstra algorithm on a weighted graph [50]. In the algorithm, sources are chosen to be the individual grid sites at the population front and sinks to be the entire collection of grid sites at  $y = 0$  since we do not, *a priori*, know which site in the founding population will be the ancestor for a given site on the final population front. The algorithm computes the shortest paths from each site at the top back to the bottom, which we collectively refer to as “fastest paths”. Edge weights are set by

$$w((i, j), (k, l)) := \frac{1}{r(i, j)} = \frac{1}{I(i, j) + 1}, \quad (4)$$

for grid site at  $(i, j)$  and neighboring node at  $(k, l)$ . Here  $r(i, j)$  is the reproduction rate at site  $(i, j)$ . Thus, the edge weights are the expected waiting times for reproduction of a deme at  $(i, j)$ , meaning that in general  $w$  will be asymmetric since the reproduction time of a site just inside a hotspot is different to the reproduction time of a neighboring site just outside of a hotspot. In practice, the asymmetry in weights is resolved by choosing a starting point at the population front, from which the search propagates outwards and downwards. The algorithm eliminates the demographic noise contribution inherent to the Eden model, thereby isolating the influence of the heterogeneous landscape on genetic lineages. Demographic noise could be reintroduced by assigning edge weights as Poisson random variables whose mean is the expected reproduction time at each deme; the resulting shortest paths would recreate Eden model lineages exactly [51].

We account for the multiplicity in fastest paths with similar arrival times by calculating, for each node at the top, the arrival time to each of the sink nodes at the bottom. We then select all paths with the ten smallest arrival times, which differ by at most 4% arrival time in our simulations. Fig. 6A,B show fastest paths (blue lines) overlaid with genetic lineage site-visitation maps for hotspot intensities  $I = 1$  and  $I = 8$ , respectively. Below these site-visitation maps, we also show survival probabilities

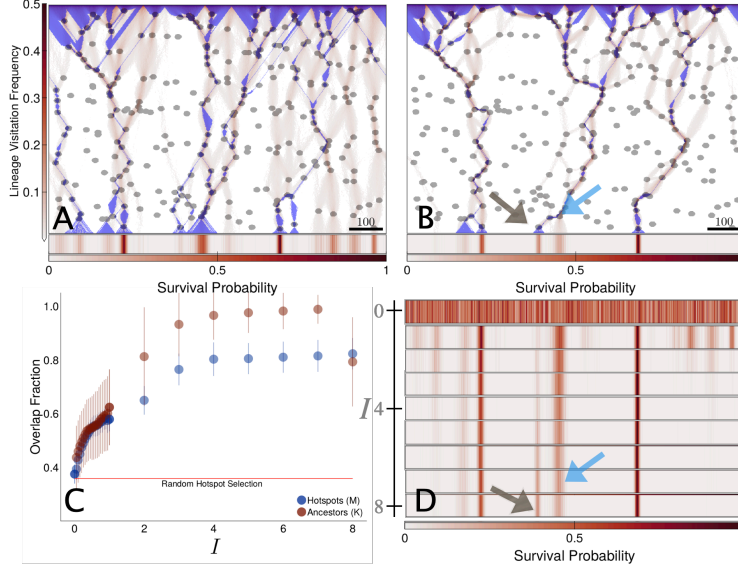


Figure 6: Environmental pinning at the end of range expansions starting from a line of occupied sites. (A, B) Genetic lineage site-visitation frequency maps at hotspot area fraction  $\phi = 0.1$  and hotspot size  $R = 10$  with (A) hotspot intensity  $I = 1$  and (B)  $I = 8$  for the same landscape. Hotspots are indicated in grey. Ancestor survival probabilities as functions of lateral position are shown beneath. Blue lines indicate fastest paths determined via the Dijkstra algorithm. (C) Overlap fraction between genetic lineages and fastest paths ( $M$ , blue markers) as well as between fastest path terminal positions and surviving ancestors ( $K$ , dark red markers). Error bars represent standard deviations. (D) Sequence of ancestor survival probabilities for hotspot intensities ranging from  $I = 0$  (top) to  $I = 8$  (bottom). Blue and gray arrows highlight an example of a trade-off between traversal distance and traversal time.

for ancestral demes as one-dimensional heatmaps indicating the probability that a given site has offspring at the front at the end of the simulation. Lineage pinning is visible at both  $I$  values. However, lineage probability distributions are much more concentrated near fastest paths for  $I = 8$ , which we describe as a “strong” pinning regime, compared to “weak” pinning at  $I = 1$ .

Due to the lattice discretization, the calculation of fastest paths generally produces a multiplicity of fastest paths, with identical travel times, from a given point at the final-time front. This degeneracy creates some two-dimensional regions of neighboring, (nearly) equal-time paths such as the blue triangles at the base of the genetic lineage trees in Figures 6A,B, one example being indicated by a gray arrow in Fig. 6B. Interestingly, these two-dimensional regions of degenerate paths predict well the location of ancestor survival probability peaks, particularly in the strong pinning regime, as discussed below.

To quantify the degree to which fastest paths predict genetic lineage structure and surviving ancestors, we examine how commonly fastest paths coincide with genetic lineages with regard to visited hotspots and with regard to tree root positions. First, we assess to what extent the subset of hotspots through which genetic lineages most often pass, as seen in Fig. 2 and Fig. 4, are a result of chance or arise due to fastest paths passing through them. To that end, we calculate the overlap fraction of visited hotspots  $m(G, S) := |G \cap S| / |G \cup S|$  where  $G$  and  $S$

are the subset of hotspots visited by genetic lineages and fastest paths in an individual simulation, respectively, and  $|\cdot|$  represents the number of elements in a set.  $M = \langle m \rangle$  denotes the average of this observable taken over our ensemble of simulations on the same landscape. Thus,  $M = 1$  when fastest paths and genetic lineages pass through the same subset of hotspots. A lower bound for  $M$  is the null expectation at  $I = 0$  (red horizontal line in Fig. 6C) for the coincidental overlap of lineages with “hotspots” that exert no influence. We calculate this lower bound for all intensities by randomly generating five different distributions of hotspots with identical size and area fraction and computing the fraction of these that are visited, per simulation, by our lineages computed from uniform landscapes.

Shown in Fig. 6C is  $M$  versus hotspot intensity  $I$ , with uncertainty bars calculated as standard deviations from our simulation ensemble. Here again, we see an increase and then a saturation behavior with increasing  $I$ , reflecting that the hotspot intensity facilitates the transition to a pinned state, here characterized by high  $M$ . Thus, at intensities above some threshold (for the parameters here  $I \approx 1.5$ ), fastest paths provide excellent predictors for the subset of visited hotspots, indicating a high correlation between fastest paths and lineages.

Returning to our observation of two-dimensional triangular regions of neighboring degenerate paths at the base of the genetic lineage trees, we now demonstrate that the

likely surviving ancestors are those which begin near one of these regions. In principle there are many degenerate paths that arise when connecting points at the front with the initial population, however we limit our scope to the more tractable problem of determining how often surviving ancestors fall within a region of the ten fastest paths that emerge as paths to the nearest hotspot from the initial population. So, for an individual simulation, we examine the fraction of surviving ancestors that lie at the base of some fastest path from the front via  $k := \frac{1}{L} \sum s(x)\rho(x)$ , where  $s(x)$  and  $\rho(x)$  are 1 if a lineage or fastest path, respectively, have a terminating position  $(x, 0)$  and 0 otherwise.  $K = \langle k \rangle$  indicates the average over our ensemble on the same landscape.

Shown in Fig. 6C is  $K$  versus hotspot intensity  $I$  at fixed hotspot area fraction and hotspot size. At  $I = 0$  fastest paths become shortest paths and hence every position  $(x, 0)$  is visited, resulting in  $K = 1$ ; hence this point is omitted. We see a trend in  $K$  similar to that of  $M$ : fastest paths and surviving ancestors are highly correlated at high intensities.

Interestingly, there is a sudden decrease in  $K$  at intensity  $I = 8$ . This drop is a consequence of the trade-off between travel distance and travel time for this particular landscape. The trade-off can be understood in terms of path optimization as follows: In uniform environments, genetic lineages have a propensity to follow shortest-distance (vertical) paths (Fig. 2A); however, hotspots disrupt this tendency by inducing paths of longer distance and shorter time, often giving rise to lateral-biased motion of lineages that follow these paths. The consequences of this trade-off can be seen by examining the ancestor survival probabilities as functions of horizontal position for hotspot intensities ranging from  $I = 0$  to  $I = 8$  (Fig. 6D): there is a gradual shift in the ancestor survival probability peak (blue arrow to gray arrow). When the hotspot intensity is low, genetic lineages tend to follow a vertical path from a prominent hotspot (marked by a blue arrow in Fig. 6B) to  $y = 0$ . As the hotspot intensity increases, lineages take a lateral excursion to a different hotspot near  $y = 0$  (gray arrow) which makes the path geometrically longer but reduces the total travel time. This shift demonstrates that increasing the hotspot intensity biases lineages towards faster optimal paths that pass through more hotspots, at the expense of larger traversal distances.

### Meandering of Lineages and of Fastest Paths

The KPZ time-scaling of genetic lineage coalescence in uniform environments is related to the superdiffusive lateral meandering of the lineage trajectories, as lineages coalesce whenever they intersect [22, 41]. Specifically, the lateral mean-squared displacement (MSD) of the lineages, parameterized by vertical distance  $l_f$  below the front, scales as  $(\text{MSD}) \sim l_f^\alpha$ ,  $\alpha = 4/3$ , whereas an exponent of  $\alpha = 1$  would indicate diffusive meandering. In this section, we examine how environmental heterogeneity

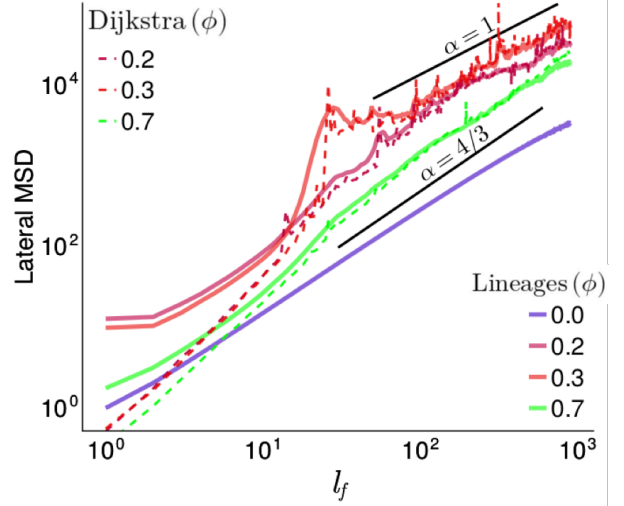


Figure 7: Lateral mean-squared displacement (MSD) of genetic lineages (solid curves) and fastest paths (dashed curves) as a function of distance  $l_f$  from the final-time population front at various  $\phi$  and fixed  $I = 7$  and  $R = 10$ . Reference lines show power-law scaling  $\text{MSD} \sim l_f^\alpha$  corresponding to diffusive (slope  $\alpha = 1$ ) and KPZ superdiffusive (slope  $\alpha = 4/3$ ) random walkers.

ity influences this lineage meandering in order to gain insight into the accelerated loss of genetic diversity.

Fig. 7 shows the lateral MSD of genetic lineages versus  $l_f$  for three different  $\phi$  values, with hotspot intensity fixed at a value of  $I = 7$ . Also plotted in Fig. 7 are MSD curves for lateral meandering of the calculated fastest paths. Strikingly, at large distances, the lateral MSD of the genetic lineages closely follows those of the fastest paths. This supports the notion that in the strong-pinning regime, lineage motion is largely dictated by fastest paths induced by the environmental structure, and thus coalescence statistics are determined by the environment rather than by demographic noise.

Both the fastest paths and the genetic lineages show qualitatively different growth of lateral MSD with lineage length at different densities. Consistent with our expectation, we observe superdiffusive growth in MSD following the KPZ expectation ( $\text{MSD} \sim l_f^{4/3}$ ) both in the absence of hotspots ( $\phi = 0$ ) and at high hotspot densities ( $\phi = 0.7$ ). The magnitude of the fluctuations is higher in the presence of hotspots, reflecting the renormalized front propagation speed in the effective medium generated by the high density of hotspots as argued in **Sector Coarsening**.

At intermediate values of  $\phi$  ( $\phi = 0.2$  and  $\phi = 0.3$  in Fig. 7) the lateral fluctuations at large distance scales deviate from KPZ scaling, signaling a qualitatively different regime when hotspots are spaced far apart and do not behave as a quasi-uniform effective medium. At these



area fractions, the lateral meandering shows growth consistent with diffusive statistics ( $\text{MSD} \sim l_f$ , compare to  $\alpha = 1$  reference line on logarithmic axes). When the pinning sites are well-separated, the hotspots are well-approximated as isolated pinning points for the genetic lineages. The fastest path can be viewed as a union of line segments connecting each hotspot to the closest hotspot in its downstream parabola of influence (Fig 1B). Since the hotspot positions are the result of a Poisson point process, each segment has a characteristic longitudinal and lateral extent, whose scaling we derive in **SI Appendix**. We hypothesize that the aggregation of many such independent segments generates a random walk in the lateral displacements of the fastest paths with the vertical direction taking the place of time, providing a mechanism for the diffusive growth of the lateral MSD observed at intermediate area fractions.

### Genetic Lineage Coalescence Rate and Common Ancestry

One important measure of the biological consequences of environmental lineage pinning is provided by the expected time  $T_2$  since common ancestry of two sampled organisms in a population. In population genetics,  $T_2$  is proportional to the expected number of pairwise nucleotide site differences between two sampled genomes, assuming a constant rate of neutral mutations [52]. Viewing genetic lineages as random motion through the environment, features of genetic structure are illuminated by the coalescence rate  $J(\tau | \Delta x_0)$  representing the probability per unit time that genetic lineages ending at two sites separated by distance  $\Delta x_0$  on the population front have a most recent common ancestor born at reverse-time  $\tau$ .

A mapping of genetic lineage motion to the theory of random walks has resulted in estimations for the asymptotic power laws in range expansions in uniform environments [41]: It was found that  $J$  depends on  $\tau$  only through the combination  $\Delta x_0/\tau^\xi$  with KPZ exponent  $\xi = 2/3$ . (Here and throughout, lengths are implicitly scaled by deme size and times by  $r_0^{-1}$ .) In particular, in the regime  $\tau/\Delta x_0^{3/2} \gg 1$ , which represents coalescence events in which lineages located nearby at the front can be traced back to a distant common ancestor, has a form

$$J(\tau | \Delta x_0) \propto \frac{1}{\Delta x_0^{3/2}} \left( \frac{\tau}{\Delta x_0^{3/2}} \right)^\gamma, \quad (5)$$

with a numerically determined exponent  $\gamma = 1.64 \pm 0.05$  for uniform landscapes [41].

Following Ref. [41], we calculate  $J$  for all lineage pairs with separation  $\Delta x_0$  at the front less than  $\Delta x_{0,\max}$ , which is kept much smaller than the system width  $L$  to avoid finite size effects. As expected, we find that when  $\Delta x_{0,\max}$  is less than the hotspot diameter  $2R$ , the coalescence rate  $J(\tau | \Delta x_0)$  reproduces the results in Ref. [41] (thus, data not shown here). For this reason, we set

$\Delta x_{0,\max} = 300$  hereafter so that  $2R < \Delta x_{0,\max} \ll L$ ; other  $\Delta x_{0,\max}$  values in this regime produced similar results. With this choice, we find that the coalescence rate takes on additional variation in the regime  $\tau/\Delta x_0^{3/2} \ll 1$  (Fig. 8A) reflecting the presence of hotspots. Even so, the  $\tau/\Delta x_0^{3/2} \gg 1$  regime retains its power-law form with similar exponent  $\gamma$  measured for various hotspot area fractions, albeit with a shift in the distribution.

With the interpretation of the hotspot landscape as an effective medium, valid for large sampling radius  $\Delta x_0 \gg 2R$ , the linear coalescence dynamics ought to resemble the uniform landscape case with some time rescaling  $\beta$ ,

$$J(\tau | \Delta x_0) \propto \frac{1}{\Delta x_0^{3/2}} \left( \frac{\beta\tau}{\Delta x_0^{3/2}} \right)^\gamma. \quad (6)$$

We estimate  $\beta$  and  $\gamma$  as a function of  $\phi$  via a linear fit with slope  $\gamma$  in the  $\tau/\Delta x_0^{3/2} \gg 1$  regime. The constant of proportionality,  $c$ , omitted from Eq. 6 is assumed to be independent of  $\phi$ , and appears in the intercept of the fit as  $\log(c\beta^\gamma)$ , with  $c$  then calculated in absence of hotspots. The inset of Fig. 8B shows the  $\gamma$  (gray circles) and  $\beta^{-1}$  (green triangles) obtained in this way. Replotting the data with time rescaled by factor  $\beta$  collapses the curves onto the uniform-environment distribution, supporting the effective-medium interpretation. Moreover, the time rescaling  $\beta$  is found to be inversely proportional to the typical hotspot separation length scale  $\lambda$  given by Eq. 3 (blue curve).

For our finite-time simulation, given that two sampled organisms at the population front at time  $t_{\max}$  have a common ancestor in the expansion history, the expected time  $T_2$  since their common ancestry is calculated from the first moment of  $J$  as

$$T_2(\Delta x_0 | \tau) = \frac{\int_0^{t_{\max}} \tau \cdot J(\tau | \Delta x_0) d\tau}{\int_0^{t_{\max}} J(\tau | \Delta x_0) d\tau}. \quad (7)$$

We calculate  $T_2$  from Eq. 7, averaged over the entire final-time population front and normalized to same the measure calculated in the uniform landscape,  $T_{2,0}$ . Fig. 9 shows  $T_2/T_{2,0}$  plotted against  $\phi$  for several hotspot intensities  $I$ . Notably,  $T_2/T_{2,0}$  exhibits a non-monotonic dependence on hotspot area fraction  $\phi$ . At low  $\phi$ , adding more hotspots shifts lineage coalescences toward more recent common ancestors, on average. However, for  $\phi$  values greater than  $\phi_c \approx 0.3$ ,  $T_2/T_{2,0}$  increases roughly linearly with  $\phi$ , with points for hotspot intensities  $I \gtrsim 1.5$  being comparable at a given  $\phi$ ; this trend with  $I$  is reminiscent of the saturation effect for genetic lineages pinned to optimal paths at similar intensities.

An extreme case (not shown in Fig. 9) is  $\phi = 1$ , in which the landscape is characterized by a uniformly increased replication rate and front propagation speed. Moreover, our system displays a duality in which, at high  $\phi$ , non-hotspot areas behave as isolated growth obstacles (regions of decreased replication rate) which genetic lineages now try to avoid. The transition between these

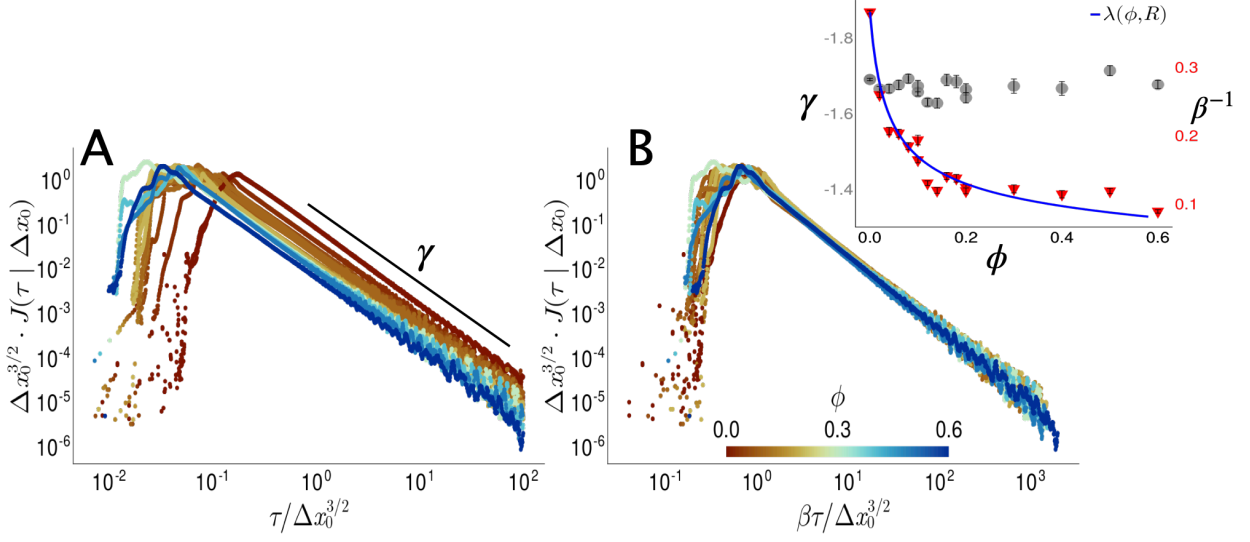


Figure 8: Log-log plot of the scaled lineage coalescence rate,  $\Delta x_0^{3/2} J(\tau | \Delta x_0)$ , for reverse-time  $\tau$  and final-time separation  $\Delta x_0$ , at  $I = 3$ ,  $R = 10$  and for various  $\phi$ , plotted against (A)  $\tau/\Delta x_0^{3/2}$  and (B)  $\beta\tau/\Delta x_0^{3/2}$ . Inset shows  $\gamma$  (circles) and  $\beta^{-1}$  (triangles) calculated from a linear fit of  $\log(\Delta x_0^{3/2} J)$  vs.  $\log(\beta\tau/\Delta x_0^{3/2})$  for  $\tau/\Delta x_0^{3/2} \gg 1$ . The horizontal colorbar indicates hotspot area fraction for the corresponding coalescence curves. Also shown is the typical hotspot separation length scale  $\lambda(\phi, R)$  (blue curve) scaled to the maximum value of  $\beta^{-1}$ .

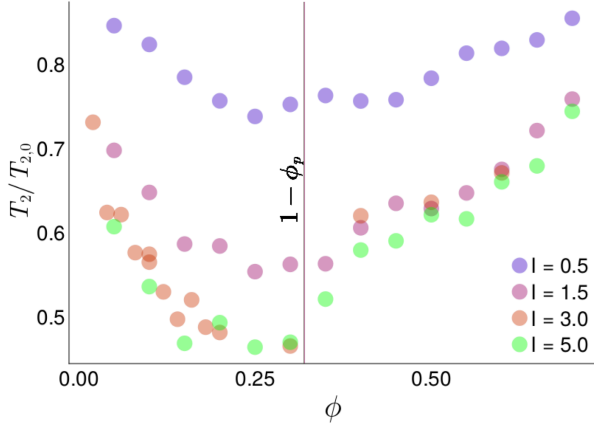


Figure 9: Mean common ancestry time  $T_2$ , normalized by that of the uniform landscape  $T_{2,0}$ , vs. hotspot area fraction  $\phi$  at different hotspot intensities  $I$ . Vertical line indicates a reference value  $1 - \phi_p \approx 0.3$ .

two dual regimes, we suggest, is related to the transition in  $T_2/T_{2,0}$  between the low  $\phi$  and high  $\phi$  behavior, which occurs near a suggestive value of  $\phi_c \approx 1 - \phi_p$ , with  $\phi_p \approx 0.68$  being the percolation transition for overlapping discs [48]. When the non-hotspot regions stop percolating at  $0.3 \lesssim \phi$ , such areas act as isolated obstacles.

## Conclusion

We have found that an environmental *pinning* effect on the genetic lineages arises in structured landscapes of hotspots, which we can understand as superdiffusive random walks that are biased toward certain optimal paths. Using the Dijkstra algorithm and viewing hotspots as geometric lenses of relative index of refraction  $v_{out}/v_{in} \sim (I + 1)^{-1}$ , we found that such optimal paths correspond to fastest paths that light would take in the analogous system. For large hotspot intensity  $I$ , these fastest paths predict much of the genetic lineage motion, including the survival probability of ancestral lineages. In such systems with strong environmental or landscape-induced noise, measures of sector coarsening reflect the intrinsic, demographic noise at short timescales and cross over to a *different* KPZ time-scaling regime determined by the environment at large timescales. A surprising non-monotonic behavior was observed in the mean time  $T_2$  since common ancestry for pairs of demes at the front as hotspot area fraction  $\phi$  was varied, indicating that  $\phi \approx 0.3$  produces fronts with the least genetic diversity.

A key manifestation of the competition between demographic and environmental noise is highlighted by our comparison of simulated lineage positions and calculated fastest paths (Fig. 6). Viewed geometrically, there is an optimal path trade-off that arises from the tendency of demographic noise to favor fluctuations around shortest-distance paths (Fig. 2A) while environmental noise pulls lineages into excursions through a consistent subset of hotspots that increase the travel distance but decrease

the travel time. At low hotspot intensity, demographic noise dominates and pulls lineages into shortest paths, resulting in many lineage tracks located away from fastest paths (Fig. 6B), as well as low overlap between hotspots visited by genetic lineages and fastest paths in Fig. 6A. At the other extreme, high-intensity hotspots cause genetic lineages to follow fastest paths with high probability (Fig. 6D). In this strong pinning regime, genetic lineage meandering is dictated almost entirely by that of the fastest paths (Fig. 7).

Furthermore, the meandering statistics of lineages in the strong-pinning regime is strongly influenced by the area fraction of hotspots (Fig. 7). At high area fractions, the lineages exhibit the wandering exponent of the KPZ class, similar to lineages in uniform environments. At low area fractions, however, the lineages exhibit diffusive meandering, which we argue arises from the statistics of accumulated hops among isolated hotspots that build up a strongly pinned lineage (see **SI Appendix**). In uniform environments with only demographic noise, diffusive meandering of lineages is obtained when front roughness is suppressed [41]. By contrast, our model exhibits a rough front, yet the meandering exponent deviates from the KPZ expectation, which shows that landscape-induced noise can decouple the wandering statistics of lineages from the roughness statistics of the front.

What does this mean for the genetic structure? Individual simulation snapshots may give the impression that growth through a landscape of hotspots produces similarly random genetic lineage trees to those in uniform environments. However, we have found that a structured environment of high-intensity hotspots pins genetic lineages to fastest paths, giving a strong deterministic component to the genetic structure of the range expansion for a given environment. This lineage pinning is associated with an accelerated loss of genetic diversity, with the implication that sites (or more generally individuals) found near one of the environmentally-determined optimal paths have the highest likelihood of influencing future genetic composition through surviving descendants. Our results suggest that, for non-neutral evolution, random hotspot landscapes may increase the importance of chance relative to selection as was seen in landscapes of obstacles [32]. Future studies could examine whether beneficial mutations are more frequently lost from the expansion when they happen to originate away from a fastest path.

The connection between lineage pinning and the non-monotonic dependence of  $T_2$  on hotspot area fraction holds intriguing potential connections to percolation theory. As shown in Fig. 9, the minimum value of  $T_2$  occurs at  $\phi \approx 0.3$  over a wide range of hotspot intensities. This raises the possibility that  $T_2$  is minimized at a universal value  $\phi = 1 - \phi_p$ , where  $\phi_p \approx 0.68$  marks the percolation transition for overlapping discs [48]. We can view  $\phi = 1 - \phi_p$  as the value at which non-hotspot regions cease to percolate as  $\phi$  is increased. This would imply

that the percolation transition of non-hotspot regions coincides with a minimization in the number of similarly fastest paths from front to ancestors, and thus a maximization of the lineage pinning effect and its associated loss of genetic diversity. In this view, lineages are biased toward fewer fastest paths, leading to more recent lineage coalescences. As  $\phi$  increases above this transition, the number of similarly fastest paths expands to eventually include all paths remaining in hotspots. Thus as we approach  $\phi = 1$ , which is again a uniform environment, the lineage-pinning effect disappears, returning lineage coalescence statistics to that of the uniform landscape albeit with an overall time rescaling.

Thus, KPZ statistics seen in uniform landscapes can also arise in structured environments, coming from demographic noise or from environmental quenched-random noise. In the absence of environmental heterogeneity, demographic noise alone determines the outcome of neutral evolution. Low intensity hotspots give rise to fastest paths through the landscape but are too weak to out-compete genetic lineage superdiffusive motion. More intense hotspots impart a sufficiently high boost in reproduction rate to portions of the population front entering a hotspot that they consistently out-compete the population remaining outside of a hotspot, producing genetic lineages bound close to the subset of hotspots defining a landscape’s fastest paths. In this lineage-pinning regime, the genetic structure of the range expansion becomes predictable, to a large degree, from the geometry of the hotspot distribution. In other words, the quenched noise of the environment replaces demographic noise as the main determinant of evolutionary dynamics.

## Acknowledgements

J.P. thanks Abhijeet Melkani for discussions about the diffusive wandering of directed polymers. J.G.N. acknowledges support from the National Science Foundation Research Traineeship in Intelligent Adaptive Systems (NSF-DGE-1633722) and the NSF-CREST Center for Cellular and Biomolecular Machines at UC Merced (NSF-HRD-1547848). J.G.N. and D.A.B. acknowledge support from the Hellman Fellows Fund.

## References

- [1] Robert E. Ricklefs and Eldredge Bermingham. “The concept of the taxon cycle in biogeography”. In: *Global Ecology and Biogeography* 11.5 (Sept. 2002), pp. 353–361. DOI: 10 . 1046 / j . 1466 - 822x . 2002 . 00300 . x. URL: <https://doi.org/10.1046/j.1466-822x.2002.00300.x>.
- [2] Carey D. Nadell, Knut Drescher, and Kevin R. Foster. “Spatial structure, cooperation and competition in biofilms”. In: *Nature Reviews Microbiology* 14.9 (July 2016), pp. 589–600. DOI: 10 .

- 1038/nrmicro.2016.84. URL: <https://doi.org/10.1038/nrmicro.2016.84>.
- [3] Joao B. Xavier and Kevin R. Foster. “Cooperation and conflict in microbial biofilms”. In: *Proceedings of the National Academy of Sciences* 104.3 (Jan. 2007), pp. 876–881. DOI: 10.1073/pnas.0607651104. URL: <https://doi.org/10.1073/pnas.0607651104>.
- [4] M. Baym et al. “Spatiotemporal microbial evolution on antibiotic landscapes”. In: *Science* 353.6304 (Sept. 2016), pp. 1147–1151. DOI: 10.1126/science.aag0822.
- [5] Marisa M. Merino, Romain Levayer, and Eduardo Moreno. “Survival of the Fittest: Essential Roles of Cell Competition in Development, Aging, and Cancer”. In: *Trends in Cell Biology* 26.10 (Oct. 2016), pp. 776–788. DOI: 10.1016/j.tcb.2016.05.009. URL: <https://doi.org/10.1016/j.tcb.2016.05.009>.
- [6] Cindy Gidoin and Stephan Peischl. “Range Expansion Theories Could Shed Light on the Spatial Structure of Intra-tumour Heterogeneity”. In: *Bulletin of Mathematical Biology* 81.11 (Dec. 2018), pp. 4761–4777. DOI: 10.1007/s11538-018-00540-6. URL: <https://doi.org/10.1007/s11538-018-00540-6>.
- [7] Kirill S. Korolev, Joao B. Xavier, and Jeff Gore. “Turning ecology and evolution against cancer”. In: *Nature Reviews Cancer* 14.5 (Apr. 2014), pp. 371–380. DOI: 10.1038/nrc3712. URL: <https://doi.org/10.1038/nrc3712>.
- [8] Elaine J. Fraser et al. “Range expansion of an invasive species through a heterogeneous landscape - the case of American mink in Scotland”. In: *Diversity and Distributions* 21.8 (Jan. 2015). Ed. by Lluís Brotons, pp. 888–900. DOI: 10.1111/ddi.12303.
- [9] Kenneth Petren and Ted J. Case. “An Experimental Demonstration of Exploitation Competition in an Ongoing Invasion”. In: *Ecology* 77.1 (Jan. 1996), pp. 118–132. DOI: 10.2307/2265661. URL: <https://doi.org/10.2307/2265661>.
- [10] Alan Templeton. “Out of Africa again and again”. In: *Nature* 416.6876 (Mar. 2002), pp. 45–51. DOI: 10.1038/416045a. URL: <https://doi.org/10.1038/416045a>.
- [11] Brenna M. Henn, L. L. Cavalli-Sforza, and Marcus W. Feldman. “The great human expansion”. In: *Proceedings of the National Academy of Sciences* 109.44 (Oct. 2012), pp. 17758–17764. DOI: 10.1073/pnas.1212380109.
- [12] Vitor Sousa, Stephan Peischl, and Laurent Excoffier. “Impact of range expansions on current human genomic diversity”. In: *Current Opinion in Genetics & Development* 29 (Dec. 2014), pp. 22–30. DOI: 10.1016/j.gde.2014.07.007.
- [13] Stephan Peischl et al. “Genetic surfing in human populations: from genes to genomes”. In: *Current Opinion in Genetics and Development* 41 (Dec. 2016), pp. 53–61. DOI: 10.1016/j.gde.2016.08.003.
- [14] Laurent Excoffier and Nicolas Ray. “Surfing during population expansions promotes genetic revolutions and structuration”. In: *Trends in Ecology & Evolution* 23.7 (July 2008), pp. 347–351. DOI: 10.1016/j.tree.2008.04.004. URL: <https://doi.org/10.1016/j.tree.2008.04.004>.
- [15] Regis Ferriere and Stéphane Legendre. “Eco-evolutionary feedbacks, adaptive dynamics and evolutionary rescue theory”. In: *Philosophical Transactions of the Royal Society B: Biological Sciences* 368.1610 (Jan. 2013), p. 20120081. DOI: 10.1098/rstb.2012.0081. URL: <https://doi.org/10.1098/rstb.2012.0081>.
- [16] Benedict Borer et al. “Spatial organization in microbial range expansion emerges from trophic dependencies and successful lineages”. In: *Communications Biology* 3.1 (Nov. 2020). DOI: 10.1038/s42003-020-01409-y. URL: <https://doi.org/10.1038/s42003-020-01409-y>.
- [17] Oskar Hallatschek and David R. Nelson. “Population genetics and range expansions”. In: *Physics Today* 62.7 (July 2009), pp. 42–47. DOI: 10.1063/1.3177227. URL: <https://doi.org/10.1063/1.3177227>.
- [18] Diana Fusco et al. “Excess of mutational jackpot events in expanding populations revealed by spatial Luria–Delbrück experiments”. In: *Nature Communications* 7.1 (Oct. 2016). DOI: 10.1038/ncomms12760.
- [19] QinQin Yu et al. “Mutability of demographic noise in microbial range expansions”. In: *The ISME Journal* 15.9 (Mar. 2021), pp. 2643–2654. DOI: 10.1038/s41396-021-00951-9.
- [20] O. Hallatschek et al. “Genetic drift at expanding frontiers promotes gene segregation”. In: *Proceedings of the National Academy of Sciences* 104.50 (Dec. 2007), pp. 19926–19930. DOI: 10.1073/pnas.0710150104.
- [21] Laurent Excoffier, Matthieu Foll, and Rémy J. Petit. “Genetic Consequences of Range Expansions”. In: *Annual Review of Ecology, Evolution, and Systematics* 40.1 (Dec. 2009), pp. 481–501. DOI: 10.1146/annurev.ecolsys.39.110707.173414.
- [22] Matti Gralka et al. “Allele surfing promotes microbial adaptation from standing variation”. In: *Ecology Letters* 19.8 (June 2016). Ed. by Bernd Blasius, pp. 889–898. DOI: 10.1111/e1e.12625.
- [23] Maxim O. Lavrentovich and David R. Nelson. “Survival probabilities at spherical frontiers”. In: *Theoretical Population Biology* 102 (June 2015), pp. 26–39. DOI: 10.1016/j.tpb.2015.03.002.

- [24] Richard A. Neher and Oskar Hallatschek. “Genealogies of rapidly adapting populations”. In: *Proceedings of the National Academy of Sciences* 110.2 (Dec. 2012), pp. 437–442. DOI: 10.1073/pnas.1213113110. URL: <https://doi.org/10.1073/pnas.1213113110>.
- [25] John Wakeley. *Coalescent Theory. An Introduction*. Roberts & Company Publishers, 2008, p. 220. ISBN: 9780974707754.
- [26] Jon F Wilkins and John Wakeley. “The Coalescent in a Continuous, Finite, Linear Population”. In: *Genetics* 161.2 (June 2002), pp. 873–888. DOI: 10.1093/genetics/161.2.873. URL: <https://doi.org/10.1093/genetics/161.2.873>.
- [27] Kimberly A. With. “The Application of Neutral Landscape Models in Conservation Biology”. In: *Conservation Biology* 11.5 (Oct. 1997), pp. 1069–1080. DOI: 10.1046/j.1523-1739.1997.96210.x. URL: <https://doi.org/10.1046/j.1523-1739.1997.96210.x>.
- [28] Kimberly A. With. “The Landscape Ecology of Invasive Spread”. In: *Conservation Biology* 16.5 (Oct. 2002), pp. 1192–1203. DOI: 10.1046/j.1523-1739.2002.01064.x. URL: <https://doi.org/10.1046/j.1523-1739.2002.01064.x>.
- [29] Jens Nullmeier and Oskar Hallatschek. “The Coalescent in Boundary-Limited Range Expansions”. In: *Evolution* (Jan. 2013), pp. 1307–1320. DOI: 10.1111/evo.12037.
- [30] Wolfram Möbius, Andrew W. Murray, and David R. Nelson. “How Obstacles Perturb Population Fronts and Alter Their Genetic Structure”. In: *PLOS Computational Biology* 11.12 (Dec. 2015). Ed. by Laurent Excoffier, e1004615. DOI: 10.1371/journal.pcbi.1004615.
- [31] Daniel A. Beller et al. “Evolution of populations expanding on curved surfaces”. In: *EPL (Europhysics Letters)* 123.5 (Oct. 2018), p. 58005. DOI: 10.1209/0295-5075/123/58005.
- [32] Matti Gralka and Oskar Hallatschek. “Environmental heterogeneity can tip the population genetics of range expansions”. In: *eLife* 8 (Apr. 2019). DOI: 10.7554/eLife.44359.
- [33] Murray Eden. “A two-dimensional growth process”. In: *Dynamics of fractal surfaces* 4 (1961), pp. 223–239.
- [34] Mehran Kardar, Giorgio Parisi, and Yi-Cheng Zhang. “Dynamic Scaling of Growing Interfaces”. In: *Physical Review Letters* 56.9 (Mar. 1986), pp. 889–892. DOI: 10.1103/physrevlett.56.889.
- [35] Oskar Hallatschek and David R. Nelson. “Gene surfing in expanding populations”. In: *Theoretical Population Biology* 73.1 (Feb. 2008), pp. 158–170. DOI: 10.1016/j.tpb.2007.08.008.
- [36] Oskar Hallatschek and David R. Nelson. “Life at the Front of an Expanding Population”. In: *Evolution* 64.1 (Jan. 2010), pp. 193–206. DOI: 10.1111/j.1558-5646.2009.00809.x.
- [37] Clarisa E Castillo and Maxim O Lavrentovich. “Shape of population interfaces as an indicator of mutational instability in coexisting cell populations”. In: *Physical Biology* 17.6 (Oct. 2020), p. 066002. DOI: 10.1088/1478-3975/abb2dd.
- [38] Maxim O Lavrentovich. “Critical fitness collapse in three-dimensional spatial population genetics”. In: *Journal of Statistical Mechanics: Theory and Experiment* 2015.5 (May 2015), P05027. DOI: 10.1088/1742-5468/2015/05/p05027.
- [39] Nikhil Krishnan, Diana Fusco, and Jacob G. Scott. “Range expansion shifts clonal interference patterns in evolving populations”. In: *bioRxiv* 794867 (Oct. 2019). DOI: 10.1101/794867. URL: <https://doi.org/10.1101/794867>.
- [40] Jayson Paulose and Oskar Hallatschek. “The impact of long-range dispersal on gene surfing”. In: *Proceedings of the National Academy of Sciences* 117.14 (Mar. 2020), pp. 7584–7593. DOI: 10.1073/pnas.1919485117.
- [41] Sherry Chu et al. “Evolution in range expansions with competition at rough boundaries”. In: *Journal of Theoretical Biology* 478 (Oct. 2019), pp. 153–160. DOI: 10.1016/j.jtbi.2019.06.018.
- [42] Wolfram Möbius et al. “The collective effect of finite-sized inhomogeneities on the spatial spread of populations in two dimensions”. In: *Journal of The Royal Society Interface* 18.183 (Oct. 2021). DOI: 10.1098/rsif.2021.0579.
- [43] Timothy Halpin-Healy and Yi-Cheng Zhang. “Kinetic roughening phenomena, stochastic growth, directed polymers and all that. Aspects of multidisciplinary statistical mechanics”. In: *Physics Reports* 254.4-6 (Mar. 1995), pp. 215–414. DOI: 10.1016/0370-1573(94)00087-j.
- [44] Daniel T Gillespie. “A general method for numerically simulating the stochastic time evolution of coupled chemical reactions”. In: *Journal of Computational Physics* 22.4 (Dec. 1976), pp. 403–434. DOI: 10.1016/0021-9991(76)90041-3.
- [45] Xiaodong Cai and Ji Wen. “Efficient exact and K-skip methods for stochastic simulation of coupled chemical reactions”. In: *The Journal of Chemical Physics* 131.6 (2009), p. 064108. DOI: 10.1063/1.3204422.
- [46] R Jullien and R Botet. “Scaling properties of the surface of the Eden model in  $d=2, 3, 4$ ”. In: *Journal of Physics A: Mathematical and General* 18.12 (Aug. 1985), pp. 2279–2287. DOI: 10.1088/0305-4470/18/12/026. URL: <https://doi.org/10.1088/0305-4470/18/12/026>.

- [47] Yukio Saito and Heiner Müller-Krumbhaar. “Critical Phenomena in Morphology Transitions of Growth Models with Competition”. In: *Physical Review Letters* 74.21 (May 1995), pp. 4325–4328. DOI: 10.1103/physrevlett.74.4325. URL: <https://doi.org/10.1103/physrevlett.74.4325>.
- [48] W. Xia and M. F. Thorpe. “Percolation properties of random ellipses”. In: *Physical Review A* 38.5 (Sept. 1988), pp. 2650–2656. DOI: 10.1103/physreva.38.2650.
- [49] S Torquato and HW Haslach. “Random Heterogeneous Materials: Microstructure and Macroscopic Properties”. In: *Applied Mechanics Reviews* 55.4 (July 2002), B62–B63. DOI: 10.1115/1.1483342. URL: <https://doi.org/10.1115/1.1483342>.
- [50] E. W. Dijkstra. “A note on two problems in connexion with graphs”. In: *Numerische Mathematik* 1.1 (Dec. 1959), pp. 269–271. DOI: 10.1007/bf01386390.
- [51] S. Roux, A. Hansen, and E. L. Hinrichsen. “A Direct Mapping between Eden Growth Model and Directed Polymers in Random Media”. In: *Journal of Physics A: Mathematical and General* 24.6 (1991), pp. L295–L300. ISSN: 0305-4470. DOI: 10.1088/0305-4470/24/6/008. (Visited on 07/10/2019).
- [52] Motoo Kimura. “The Rate of Molecular Evolution Considered From the Standpoint of Population Genetics”. In: *Proceedings of the National Academy of Sciences* 63.4 (Aug. 1969), pp. 1181–1188. DOI: 10.1073/pnas.63.4.1181.

## SI Appendix

### Parabolic Description of Sector Boundary Induced by Single Hotspot

As described in the main text, a single hotspot generates sector boundaries that are well described by a parabola. Approximating the effect of a hotspot on genetic sectors as a superposition of a traveling plane wave and an expanding spherical wave gives a parabola with the form  $y = ax^2 + \delta$ , where  $a = (I + 1)/4IR$  is calculated from Ref [42], and  $\delta = RI/(I + 1)$  is the vertex of the parabola below the hotspot origin. Explicitly, sector boundaries from single hotspots have the heuristic description

$$y = \frac{I + 1}{4IR}(x - h_x)^2 + h_y - R\frac{I}{I + 1}, \quad (8)$$

where  $(h_x, h_y)$  is the position of the hotspot's center. Fig. 10 shows the sector formed by a single hotspot that is well described by Eq. 8 (red curve). Also shown is a parabola with identical parameters albeit with vertex set to the center of the hotspot (black curve). We find that the placement of the parabola's vertex according to the shift  $\delta$  better describes the sector boundaries near the hotspot; however  $\delta$  has little effect on the long-time description of the parabolic sector boundaries.

### Statistics of fastest paths in the strong pinning regime at low hotspot area fractions

As seen in the main text, in the regime of strong pinning (hotspot intensity  $I \gg 1$ ), the true lineages closely follow the fastest paths identified by the Dijkstra algorithm. These paths connect frequently-visited hotspots via segments that approximate straight line segments on the lattice. At low hotspot area fraction, the hotspots can be approximated as points of vanishing size that pin the ends of the lineage segments and provide a reduction in traversal time compared to unpinned segments of the same length. The fastest path associated with an individual sampled at the front is then the collection of segments that connects that individual to a member of the ancestral demes at height zero in the shortest net traversal time.

The lateral wandering of shortest paths reflects a trade-off between tracing a perfectly vertical path (which minimizes the time taken to advance vertically on the background) and passing through randomly placed hotspots (each of which provides a fixed reduction in the traversal time). The characteristic length scales governing this trade-off can be obtained from the geometric optics calculation of Ref. [42] and are sketched in Figure 11. Consider tracing a path forward in time from the ancestral demes towards the population front. After the path has passed through a hotspot, the region of influence of that hotspot advances as the parabola  $y = ax^2$  with the parameter  $a$  determined by the hotspot intensity and radius (see Fig. 1B and Eq. 2 in main text). For the path to encounter another hotspot, the front must advance by a distance  $\ell$  whose magnitude is set by requiring that the number of hotspots in the parabolic region of height  $\ell$  and width  $\sim \sqrt{\ell/a}$  is of order one. Since hotspots are distributed as a Poisson point process with spatial density  $\rho$ ,  $\ell$  has a characteristic size governed by the relation

$$\rho\ell\sqrt{\frac{\ell}{a}} \sim 1 \Rightarrow \ell \sim a^{1/3}\rho^{-2/3}. \quad (9)$$

The subsequent segment of the fastest path is determined by the same criterion, with the newly encountered hotspot serving as the basal point of the next parabolic region.

In the limit of well-separated hotspots, the fastest paths are built up from segments whose extent in both directions is a stochastic variable, but with a characteristic height of order  $\ell$  and a typical lateral distance of order  $\sqrt{\ell/a}$ . Each segment advances upwards in the vertical direction; however, the sign of the lateral displacement is random for each segment. Since the leading scaling of the total path length is linear in the vertical displacement, the existence of characteristic sizes for the vertical and lateral displacements suggests that the lateral wandering of the path will follow a diffusive random walk with the vertical dimension  $l_f$  serving as the "time" variable. At scales  $l_f \gg \ell$ , the lateral MSD of the fastest paths is therefore expected to grow as  $\sim Dl_f$ , where the scaling of the diffusion constant  $D$  is determined by the typical vertical and horizontal step sizes:  $D \sim (\sqrt{\ell/a})^2/\ell = 1/a$ . In Fig. 7 in the main text, the measured lateral MSD of fastest paths for populations in the strong pinning regime is shown to be consistent with diffusive statistics at low and intermediate area fractions, when the hotspots are well-separated relative to their radius.

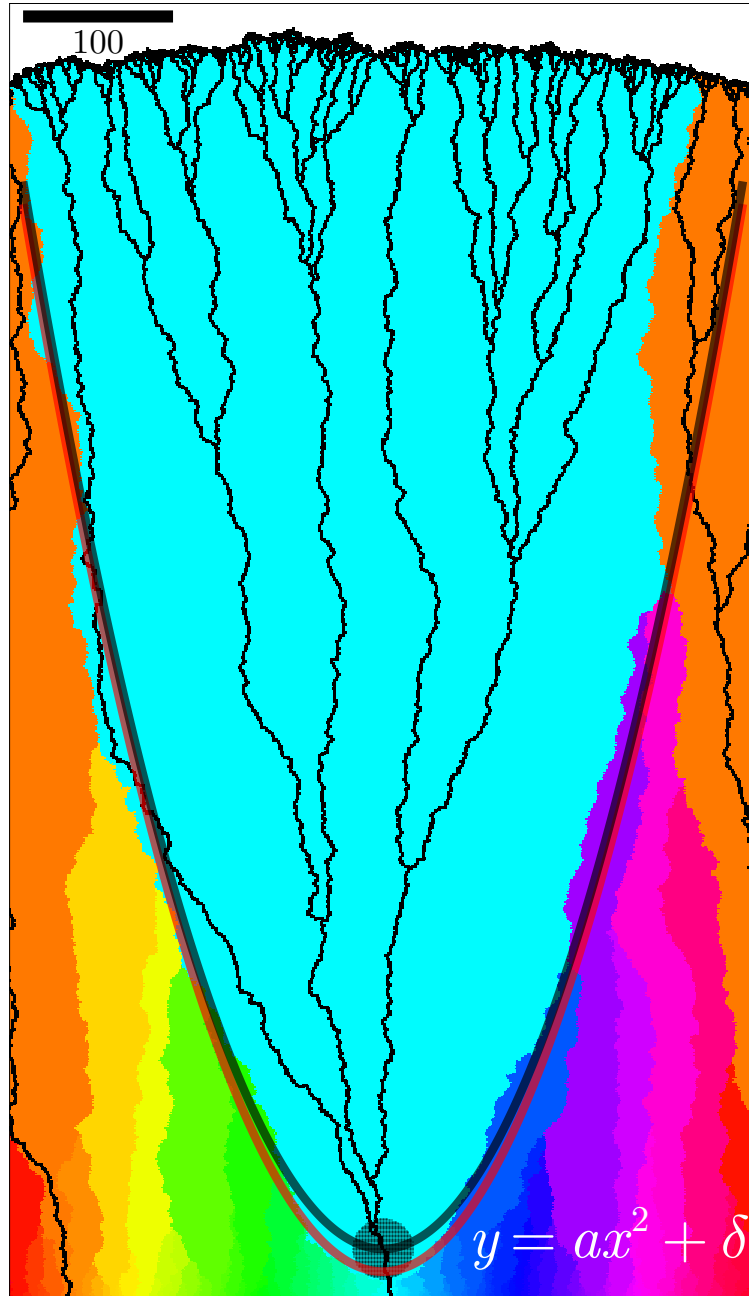


Figure 10: Illustration of Eden model for range expansion beginning as a single line at  $y = 0$  and proceeding through a heterogeneous landscape with a single hotspot, and with each color representing a distinct ancestral deme. Genetic lineages are shown as black lines. Parabolic predictions for the sector boundary induced by the hotspot are shown (red and black curves) with  $\delta = RI/(I + 1)$  and  $\delta = 0$ , respectively.



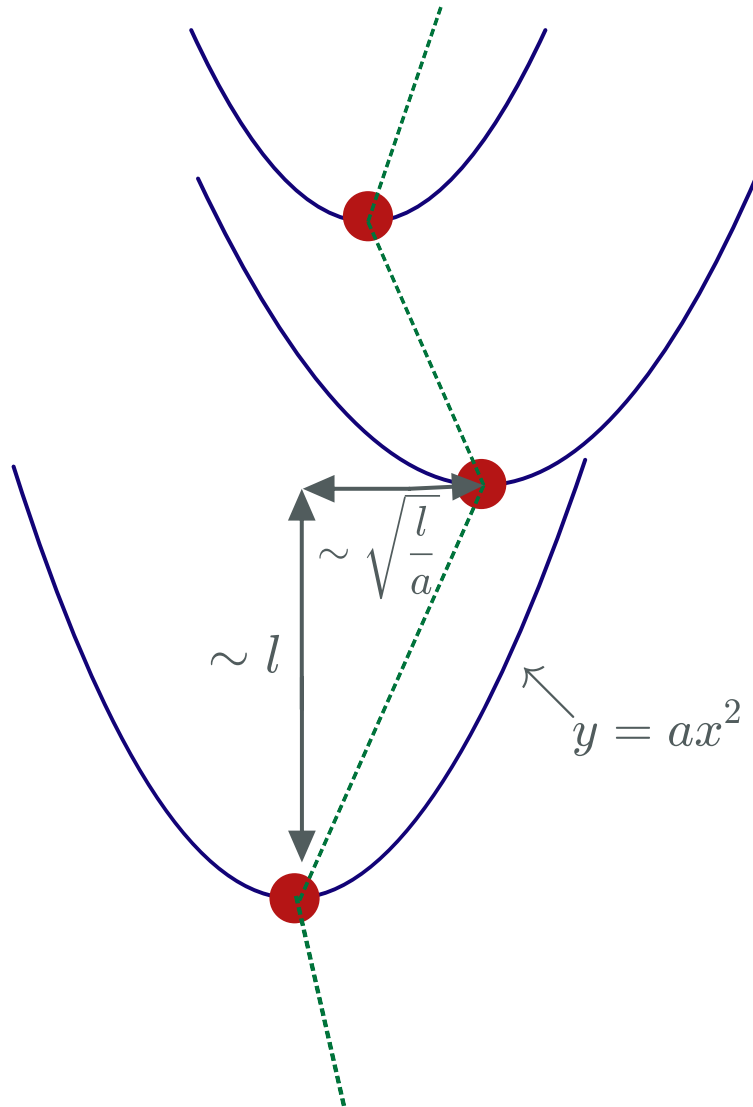


Figure 11: Sketch of approximation to meandering fastest paths in the strong pinning regime at low area fraction. The fastest path is approximated as straight segments (green dashed lines) connecting hotspots traversing the environment from bottom to top. Hotspots are drawn as discs, but are assumed to be points of vanishing size in the approximation. Each subsequent hotspot must lie in the parabola of influence (blue curve) of the current pinning point as the front advances. The vertical and lateral distances to the subsequent hotspot are both stochastic variables, but with characteristic sizes  $\ell$  and  $\sqrt{\ell/a}$  respectively.